Research on Ground of Penetrating Radar in the Coal Mine Detecting: A Case Study of Application in Huaibei Coal Mine

Yongsheng Ma[1,2], Jinsong Shen[1], Benyu Su[3, *], Yanyan Ma[2], Qilong Sun[2]
[1]*Department of Geophysics, China University of Petroleum-Beijing, 18 Fuxue Road, Changping, Beijing 102249, China*
[2]*Oil and Gas Survey CGS, Runyu Building, No. 10, Xiaoguan Dongli, Anwai, Chaoyang District, Beijing, China*
[3]*China University of Mining and Technology, No. 1, Daxue Road, Xuzhou, Jiangsu, China*
subenyu@cumt.edu.cn

***Abstract*—Although many geophysical techniques have been used to detect the disaster geological anomalous body in the Huaibei coal mine company, there are still many mining disasters happening. The main reason is that the coal seam is rich of water in Huaibei coal areas. If the ground water connects with tunnels, it will cause the flood to collapse the coal seam. However, these dangerous geological bodies usually are very hided from the viewpoint of traditional electromagnetic and seismic methods. Due to the great difference of permittivity between the water-bearing rock and the surrounding rock, the high frequency electromagnetic wave can be received by a Ground Penetrating Radar (GPR) to detect the water-bearing rocks. Hence, we try to employ the high frequency electromagnetic wave to detect the water-bearing rock, which frequently results in a coal mining disaster. Firstly, the numerical simulations based on the theory research and its` effectivity analysis are done. Then, the method is used for the coal mine of Huaibei Company. Finally, the comparison between the detected results and the geological drilling information indicates the detection effectiveness of the GPR (Ground Penetrating Radar) in the coal mine tunnel.**

***Index Terms*—Ground penetrating radar; Numerical simulation; Coal mine; Mine safety.**

I. INTRODUCTION

The Huaibei coal mine field is located in Huaibei city, Anhui province as shown in Fig. 1. In the past 10 years, there have been many incidents of water inrush and flooding. During some serious accidents, the mining area in the Huaibei coal mine field flooded totally. Many locations of these accidents caused by conducted water collapse column are the coal mine work face and the head of roadway tunneling. The main reason is that collapse column can conduct Ordovician limestone water to tunnel and this may result in a great disaster for a coal mine. Hence, the research on collapse column has been a hot point in the mine hydrogeology. Although researchers [1]–[3] have done a lot of geophysical work, still there is more work needs to be done, e.g., most of the collapse columns develop under the coal seam floor and, in this case, most seismic energy is reflected into by the roof of the Earth . Hence, the ground surface seismic method has a great challenge to detect a collapse column. Besides, basing on the electrical characteristics of collapse column, some geophysicists try to detect it by using radio wave perspective technology and mine transient electromagnetic detection technology. However, the radio wave perspective technology employs low frequency electromagnetic wave, which means that these two methods have low resolution, so that they cannot detect the small volume collapse column. Although Transient Electromagnetic Method (TEM) is the most popular geophysical method [4]–[7] for exploring geological structure in the coal tunnel, it has a blind zone of 20 meters near the transmitter area [8]. However, the Ground Penetrating Radar (GPR) can overcome the two mentioned disadvantages of the geophysical method. Application of the Ground Penetrating Radar has a long history [9] which can be widely used in different areas of engineering [10], [11].

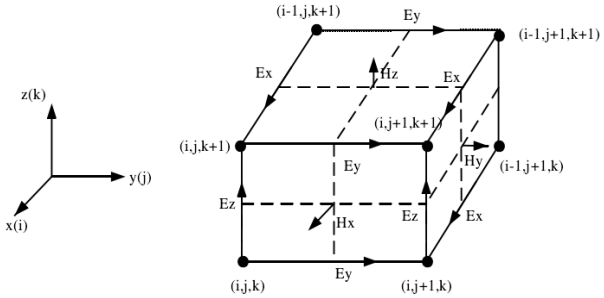

Fig. 1. Staggered mesh of finite difference.

GPR is a geophysical method which employs high frequency wave (10 MHz–10 GHz) to detect the buried geological bodies. The transmitter antenna generates high frequency electromagnetic pulses, which will be propagated in the earth. If geological anomalous bodies do exist in the earth, the electromagnetic wave will reflect them and the reflected wave will be received by the receiving antenna. The

Manuscript received 1 February, 2019; accepted 25 June, 2019.
This research was funded by a grant (No. 2018YFC0807804-02) from the National key research and development program of China and (No. BK20181360) Natural science foundation of Jiangsu Province.

structure and physical property of geological bodies can be estimated basing on the characteristics of amplitude, wave shape, and frequency [12]. Besides, compared with other geophysical methods, GPR is easier to be implemented and provides higher resolution. Hence, it is very popular in the area of engineering exploration.

There are only few papers or public reports published on the application of GPR in the coal mining. However, many papers and public reports are published for to interpret that GPR can successfully detect the ground cavity [13], [14], ground water paleochannels [15] and mapping subsurface structure [16]–[19]. Hence, in principle, GPR owns the capacity to detect the collapse column and evaluate the water-bearing. But in order to easily recognize the geological anomalous bodies, it is very necessary to process the raw data by different processing methods [20]–[23].

It is well known that the mine water is one of the main hazards in the coal mining. Besides, the relative permittivity of the coal seam is 3.4 and the relative permittivity of water is 81. Moreover, the velocity of the electromagnetic wave in the coal mine is three times of that in the collapse column containing water. Hence, there is a great wave impedance difference at the boundaries between the coal seam and the collapse column. The principle shows that the greater difference in the wave impedance is the better detecting effects are.

II. METHODOLOGY

Maxwell's equations used to describe the propagation of electromagnetic wave can be expressed in Cartesian coordinate system [24]:

$$\frac{\partial H_z}{\partial y}-\frac{\partial H_y}{\partial z}=\varepsilon\frac{\partial E_x}{\partial t}+\sigma E_x, \tag{1}$$

$$\frac{\partial H_x}{\partial y}-\frac{\partial H_z}{\partial x}=\varepsilon\frac{\partial E_y}{\partial t}+\sigma E_y, \tag{2}$$

$$\frac{\partial H_y}{\partial x}-\frac{\partial H_x}{\partial y}=\varepsilon\frac{\partial E_z}{\partial t}+\sigma E_z, \tag{3}$$

and:

$$\frac{\partial E_z}{\partial y}-\frac{\partial E_y}{\partial z}=-u\frac{\partial H_x}{\partial t}, \tag{4}$$

$$\frac{\partial E_x}{\partial z}-\frac{\partial E_z}{\partial x}=-u\frac{\partial H_y}{\partial t}, \tag{5}$$

$$\frac{\partial E_y}{\partial x}-\frac{\partial E_x}{\partial y}=-u\frac{\partial H_z}{\partial t}. \tag{6}$$

In the two domain, the electromagnetic problem can be solved by supposing $\partial/\partial z=0$.

For TE wave, the above-mentioned equations can be simplified as follows:

$$\frac{\partial H_z}{\partial y}=\varepsilon\frac{\partial E_x}{\partial t}+\sigma E_x, \tag{7}$$

$$-\frac{\partial H_z}{\partial x}=\varepsilon\frac{\partial E_y}{\partial t}+\sigma E_y, \tag{8}$$

$$\frac{\partial E_y}{\partial x}-\frac{\partial E_x}{\partial y}=-\mu\frac{\partial H_z}{\partial t}. \tag{9}$$

For TM wave, the above-expressed equations can be simplified as follows:

$$\frac{\partial E_z}{\partial y}=-\mu\frac{\partial H_x}{\partial t}, \tag{10}$$

$$\frac{\partial E_z}{\partial x}=\mu\frac{\partial H_y}{\partial t}, \tag{11}$$

$$\frac{\partial H_y}{\partial x}-\frac{\partial H_x}{\partial y}=\varepsilon\frac{\partial E_z}{\partial t}+\sigma E_z. \tag{12}$$

Eqs. (1)–(12) are the basis of FDTD (finite-different time-domain). Hence, the rectangular grid is employed to mesh the whole space and grid nodes conform to the corresponding integer label as shown in Eq. (13)

$$(i,\ j,\ k)=(i\Delta x,\ j\Delta y,\ k\Delta z). \tag{13}$$

Therefore, function $F(x, y, z, t)$ in $n\nabla t$ time can be written as

$$F^n(i,\ j,\ k)=F(i\Delta x,\ j\Delta y,\ k\Delta z,\ n\Delta t). \tag{14}$$

Here, Δx, Δy, and Δz indicate the spatial step in x, y, and z direction and Δt represent the time step. In FDTD algorithm, the expression of (14) can be written using the following

$$\frac{\partial F^n(i,\ j,\ k)}{\partial x}=\frac{F^n(i+\frac{1}{2},\ j,\ k)-F^n(i-\frac{1}{2},\ j,\ k)}{\Delta x}+O(x^2). \tag{15}$$

In Yee's meshing method technique, the relation between the electric and magnetic fields as shown in Fig. 1 is described. The E and H components of the electromagnetic field alternate and surround each other. It is the distribution characteristics of this law that makes it possible to simulate the propagation of electromagnetic waves using a computer.

According to Yee finite difference method, the distribution of space joint and time step can be decided as shown in Table I. The table describes the relationship between the integer and half-integer steps.

TABLE I. DISTRIBUTION OF SPACE JOINT AND TIME STEP.

EM field		Space sample		Time sample
		Coordinate in Y-direction	Coordinate in Y-direction	
TE	Hz	i + 1/2	j + 1/2	n + 1/2
	Ex	i + 1/2	j	n
	Ey	i	j + 1/2	n
TM	Ez	i	j	n
	Hx	i	j + 1/2	n + 1/2
	Hy	i + 1/2	j	n + 1/2

A. Stability Condition

The spatial step size (Δx, Δy, Δz) does not exist independently and it is related to the time step Δt. In order to ensure the convergence and stability of the solutions of the

discrete equations, we must find the relationship between the spatial step and the time step.

Assuming the space being lossless and the magnetic field vector being normalized, $\sqrt{\mu/\varepsilon}\,H \to H$, the corresponding Maxwell's equations are expressed as follows:

$$\nabla \times H = \frac{1}{c}\frac{\partial E}{\partial t}, \tag{16}$$

$$\nabla \times E = -\frac{1}{c}\frac{\partial H}{\partial t}, \tag{17}$$

where $c = \frac{1}{\sqrt{\mu\varepsilon}}$.

The stability of the equations should meet the requirements

$$\Delta t \le \frac{1}{c\sqrt{\frac{1}{\Delta x^2}+\frac{1}{\Delta y^2}+\frac{1}{\Delta z^2}}}. \tag{18}$$

For example, when $\Delta x = \Delta y = \Delta z$, the time step has to meet the requirements $\Delta t \le \frac{\Delta x}{c\sqrt{3}}$. When the three steps are not equal to each other, Δt should meet the requirements

$$\Delta t = \frac{\min(\Delta x_{\min}, \Delta y_{\min}, \Delta z_{\min})}{2c}. \tag{19}$$

B. Boundary Conditions

Electromagnetic waves propagate in all directions in the underground space. Although the underground space is endless, we have to consider the boundary conditions in the numerical simulation due to limited computer storage. Compared with other boundary conditions, the perfect matching layer (PML) boundary condition is employed to absorb the electromagnetic wave in the boundary area [25].

Here, we only consider the situation of TE wave and do the numerical situation by the finite difference method [24]. In order to obtain the high resolution data, we usually chose the Ricker wavelet as the source to generate signal as shown in Fig. 2.

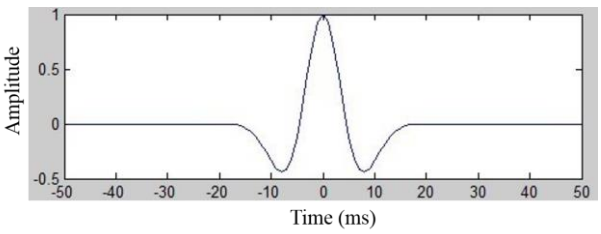

Fig. 2. The shape of wavelet in numerical simulation.

III. NUMERICAL SIMULATION OF CONCEALED GEOLOGICAL STRUCTURES

Hided collapse column is a great risk to conduct water into mine tunne. In order to study the collapse column responses of GPR, we build the geological model as shown in Fig. 3. The thickness of the coal seam is 100 meters and the area of the hazard geological body is 30 meters by 40 meters. In order to describe the geological model clearly, the horizontal slice is cut from Fig. 3 shown in Fig. 4. According to the test data from coal, the permittivity of coal seam is 3.4 and the resistivity is 2000 ohm-m. Moreover, the permittivity of the hided collapse column containing water is 75, and the resistivity of the geological body is 10 ohm-m. Suppose that we put the shield antenna on the tunnel wall as shown in Fig. 3 and the white points (see Fig. 3 also) indicate the measured points. We extract the modelling data from 3D volume as it is shown in Fig. 5.

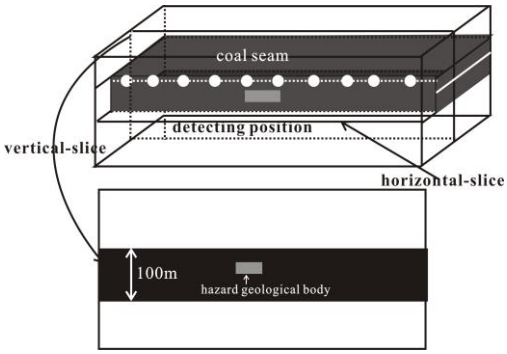

Fig. 3. Geological model of mining geology.

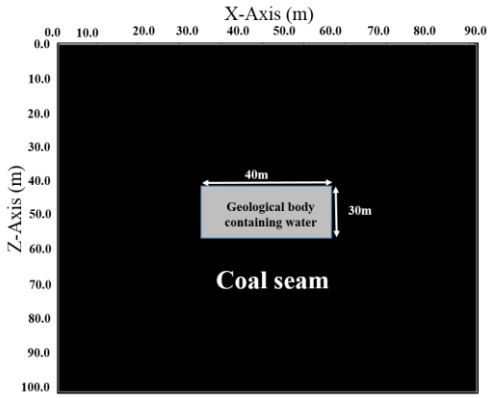

Fig. 4. The result of numerical simulation.

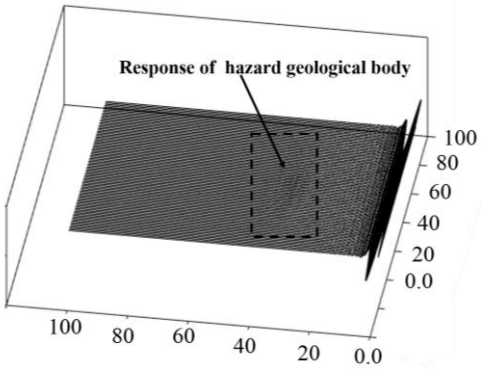

Fig. 5. The result of numerical simulation.

Although we can see the hyperbolic curve appear in Fig. 5, the resolution is not good enough to recognize that it exists. In order to recognize the position of hazard geological body easily, we should improve its resolution by the Kirchhoff integral migration.

In the uniform medium, the electric field E satisfies the wave equation

$$\frac{\partial^2 E}{\partial x^2}+\frac{\partial^2 E}{\partial y^2}+\frac{\partial^2 E}{\partial z^2}-k^2\frac{\partial E}{\partial t}=0, \tag{20}$$

where k is the propagation constant related with wave velocity and electric field E, which is located on the point p(x_p, y_p, z_p) closed by infinitely large hemisphere, can be expressed by equation (21), which is the Kirchhoff integral solution

$$E(x_p, y_p, z_p, t) = \\ = \frac{1}{2\pi}\iint_{S1}[\frac{\partial}{\partial n}(\frac{1}{r}) - \frac{1}{\upsilon r}\frac{\partial r}{\partial n}\frac{\partial}{\partial t}]\times \\ \times E(x, y, 0, t - \frac{r}{v})dS_1. \quad (21)$$

where $r = [(x - x_p)^2 + (y - y_p)^2 + (z_p)^2]^{\frac{1}{2}}$ and the normal direction of the surface $\frac{\partial}{\partial n} = -\frac{\partial}{\partial z}$.

When actually performing migration processing, the measurement data is defined on the z = 0 plane and the electric field to be determined should be ahead of the record point on the z = 0 plane. Hence, $E(x, y, 0, t - \frac{r}{v})$ in the (21) should be modified to $E(x, y, 0, t + \frac{r}{v})$.

Accordingly, the equation (21) should be rewritten to equation (22) as follows

$$E(x_p, y_p, z_p, t) = \frac{1}{2\pi}\iint_{S1}[\frac{\partial}{\partial n}(\frac{1}{r}) - \frac{1}{\upsilon r}\frac{\partial r}{\partial n}\frac{\partial}{\partial t}]\times \\ \times E(x, y, 0, t + \frac{r}{v})dS_1. \quad (22)$$

The purpose of the GPR data processing is transforming raw data to be zero offset. Hence, we should rewrite the equation (22) to equation (23) in order to get the electric field at the depth of *z*

$$E(x_p, y_p, z_p, t) = \frac{1}{2\pi}\iint_{S1}[\frac{\partial}{\partial n}(\frac{1}{r}) - \frac{1}{\upsilon r}\frac{\partial r}{\partial n}\frac{\partial}{\partial t}]\times \\ \times E(x, y, 0, \frac{2r}{v})dS_1. \quad (23)$$

Given $T = {2z_p}/{v}$, $t_0 = {2r}/{v}$, and

$$\frac{\partial}{\partial n} = -\frac{\partial}{\partial z} = -\frac{z_p}{r} = -\upsilon T/2r\,\frac{\partial}{\partial n}(\frac{1}{r}) = \frac{vT}{2r^3}, \quad (24)$$

the $E(x, y, 0, \frac{2r}{v})$ derivation of *t* can be expressed in different form as shown in equation (25)

$$\frac{\partial}{\partial t}E(x, y, 0, t_0) = \\ = \frac{E(x_p, y, 0, t_0 + \Delta t) - E(x_p, y, 0, t_0 - \Delta t)}{2\Delta t}. \quad (25)$$

Hence, equation (23) can be modified into equation (26)

$$E(x_p, y_p, z_p, 0) = \\ \frac{T}{\Delta t}\times\frac{1}{\upsilon^2 t^2}[E(x, y, 0, t_0 + \Delta t) - \\ = \frac{1}{2\pi}\iint_{S1} -E(x, y, 0, t_0 - \Delta t) + \quad dxdy, \quad (26) \\ + \frac{2\Delta t}{t_0}E(x, y, 0, t_0)]$$

where Δx, Δy, and Δz are the spatial steps in *x*, *y*, and z directions, respectively. Then, $x_p = m\Delta x$, $y_p = n\Delta y$, and $z_p = l\Delta z$, the distance between r, can be expressed by formula $r = [((m-\alpha)\Delta x)^2 + ((n-\beta)\Delta y)^2 + (l\Delta z)^2]^{1/2}$.

Discrete form of Formula (26) can be written by Formula (27) which can be employed to do Kirchhoff integral migration to process the measured data

$$E(m, n, l, 0) = \\ [E(\alpha, \beta, 0, t_0 + \Delta t) - \\ = \frac{T}{2\pi\nabla t v^2 t_0^2}\sum_{\alpha}\sum_{\beta} -E(\alpha, \beta, 0, t_0 - \Delta t) + \Delta x\Delta y. \quad (27) \\ + \frac{2\Delta t}{t_0}E(\alpha, \beta, 0, t_0)]$$

For the modelling data, as shown in Fig. 5, we process it by the Kirchhoff integral migration method. The result after the processing is shown in Fig. 6. When comparing with Fig. 5, we can see that the resolution improves a lot and, particularly, the position of geological body can be located in the coal seam.

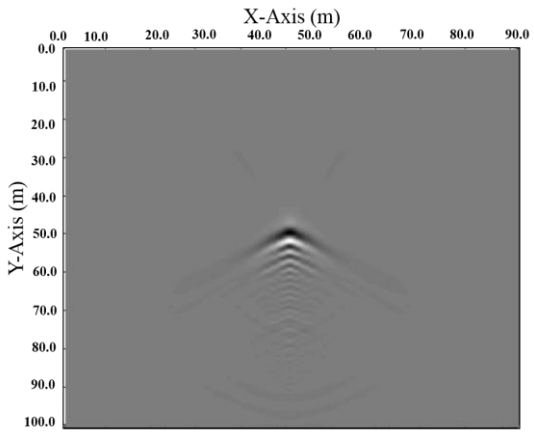

Fig. 6. Processed data by Kirchhoff Integral Migration technology.

IV. FIELD WORK

The field work was implemented in the coal field of Wuliguo, which belongs to Huaibei Mining Group Co., Ltd., which is located in the Anhui province as shown in Fig. 7.

According to the characteristics of coal distribution in China, we classify it into two parts: the west part and the east part. In the east, the coal seam is especially rich in ground water. The water hazard resulted in a serious accident in Huaibei Mining company. Hence, the coal mine company

cares a lot about the water hazard. The purpose of the field work is to locate the position of the collapse column, which usually conducts water to the tunnel. This kind of detection by using the GPR is the first time in Huaibei Mining Company and, in order to verify its effectiveness, we chose several known geological targets to do the test.

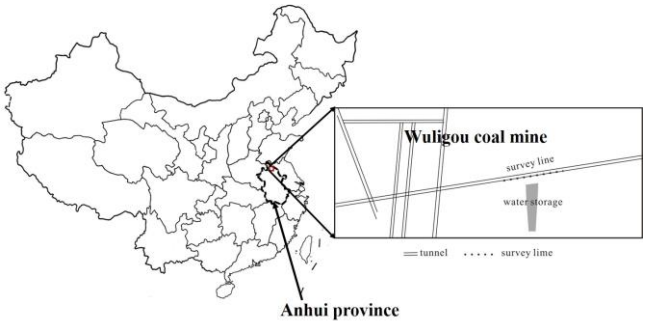

Fig. 7. The location of the coal mine for the field work.

According to the requirements of coal field, the detection was performed twice. Firstly, in order to test the effectiveness, the known geological body was detected as a target to do the test. We chose an abandoned tunnel as the target of detecting the underground coal mine. Now, the abandoned tunnel is used to store water and profile of the tunnel as shown in Fig. 8. The black points in Fig. 8 indicate the survey line and the grey area of the trapezoid indicates the water storage. Figure 9 is our final processed result. In order to show the detecting results obviously, we usually adopt the colorized picture as shown in Fig. 9.

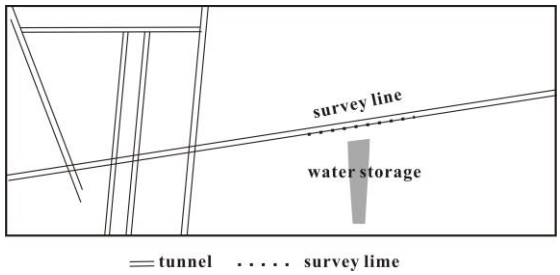

Fig. 8. The distribution of the underground tunnel in the Wuligou coal mine and the location of the abandoned tunnel as a water storage.

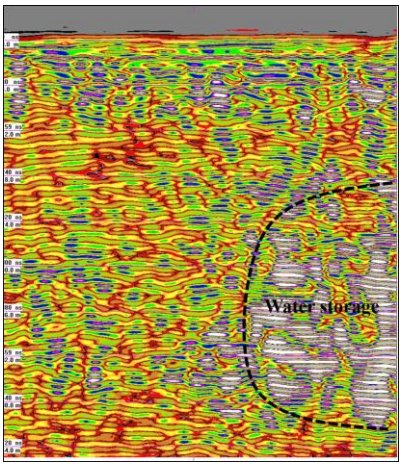

Fig. 9. The GPR detection result in the Wuligou coal mine.

We compared the detection result and the distribution position of the abandoned tunnel and we can easily conclude that the anomalous area in Fig. 9 corresponds to the water storage as shown in Fig. 8.

Besides, for detecting, we chose the other coal mine in Wuligou cole mine and the tunnel distribution is shown in Fig. 10. The purpose of detecting is to examine small geological structure, e.g., small faults in the work face. The dotted line in Fig. 10 is a survey line. The detecting results are shown in Fig. 11. From the modelling results shown in Fig. 11, we can find out that the area closed by the dotted line shows the discontinuous characteristics of the lineups, which means that there is an anomalous geological body in the work face. Based on the detection results, we acquire the geological information by the drilling technique. By comparison with the GPR detection result and the drilling result, it is indicated that GPR can really detect the anomalous structure geological body in the coal seam.

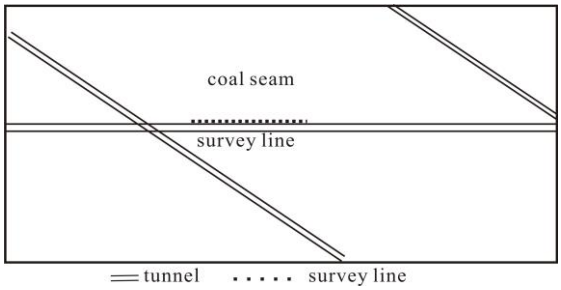

Fig. 10. The distribution of the underground tunnel in the coal mine.

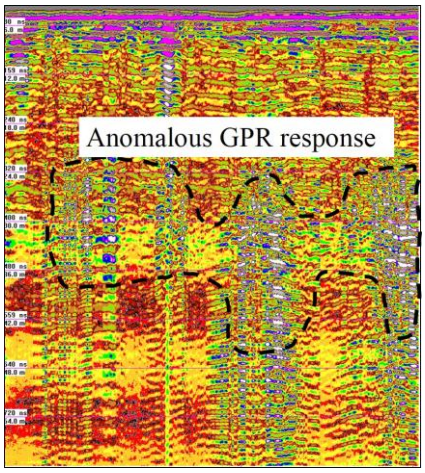

Fig. 11. The GPR detection result in the Wuligou coal mine.

V. CONCLUSIONS

In this study, to detect the hided disaster-causing geological body, GPR method is used for the first time. Both of the theory numerical modelling result and the field work indicate that GPR method is very effective to detect the hided geological body. However, the resolution of raw data cannot show the position clear enough. In order to enhance the resolution, we introduce the Kirchhoff Integral Migration technology to process data, so that we could interpret the procedure of the Kirchhoff Integral Migration method.

In the procedure of the research, the field work was carried out twice and the detecting results were verified by the known geological information or drilling geological information. However, this research is just one brand new attempt and, if the method is widely applied in the coal mine in China, we should do even more field work for to, finally, conclude its rules.

ACKNOWLEDGMENT

We are grateful to the anonymous reviewers of this paper.

REFERENCES

[1] B.-Y. Su and J.-H. Yue, "Research of the electrical anisotropic characteristics of water-conducting fractured zones in coal seams", *Applied Geophysics*, vol. 14, no. 2, pp. 216–224, 2017. DOI: 10.1007/s11770-017-0620-2.

[2] B. Su, J. Ju, and C. Sheng, "Maxwell-equations based on mining transient electromagnetic method for coal mine-disaster water detection", *Elektronika ir Elektrotechnika*, vol. 23, no. 3, pp. 20–23, 2017. DOI: 10.5755/j01.eie.23.3.18326.

[3] B. Su, J. Ju, and C. Sheng, "Borehole electromagnetic method for exploration of coal mining goaf", *Elektronika ir Elektrotechnika*, vol. 22, no. 4, pp. 37–40, 2016. DOI: 10.5755/j01.eie.22.4.15913.

[4] J. Chang, J. Yu, and B. Su, "Numerical simulation and application of mine TEM detection in a hidden water-bearing", *Journal of Environmental and Engineering Geophysics*, vol. 22, no. 3, pp. 223–234, 2017. DOI: 10.2113/JEEG22.3.223.

[5] J. Yu, R. Malekian, J. Chang *et al*., "Modeling of whole-space transient electromagnetic responses based on FDTD and its application in the mining industry", *IEEE Transactions on Industrial Informatics*, vol. 13, no. 6, pp. 2974–2982, 2017. DOI: 10.1109/TII.2017.2752230.

[6] N. Zhou, G.-Q. Xue, D.-Y. Hou, and Y. Lu, "An investigation of the effect of source geometry on grounded-wire TEM surveying with horizontal electric field", *Journal of Environmental and Engineering Geophysics*, vol. 23, no. 1, pp. 143–151, 2018. DOI: 10.2113/JEEG23.1.143.

[7] G.-Q. Xue, W. Chen, N.-N. Zhou, H. Li, "Short-offset TEM technique with a grounded wire source for deep sounding", *Chinese Journal of Geophysics*, vol. 56, no. 1, pp. 255–261, 2013. DOI: 10.6038/cjg20130126.

[8] L. Xiu, G.-Q. Xue, and Ch. Yin, "Development and Prospect of Transient Electromagnetic Method", 2017. DOI: 10.1007/978-981-10-2708-6_1.

[9] W. W.-L. Lai, X. Dérobert, and P. Annan, "A review of ground penetrating radar application in civil engineering: A 30-year journey from locating and testing to imaging and diagnosis", *NDT & E International*, vol. 96, pp. 58–78, 2017. DOI: 10.1016/j.ndteint.2017.04.002.

[10] J. L. Porsani and W. A. Sauck, "Ground-penetrating radar profiles over multiple steel tanks: Artifact removal through effective data processing", *Geophysics*, vol. 72, no. 6, pp. 210–222, 2007. DOI: 10.1190/1.2783412.

[11] R. Arutunyan, L. Bolshov, and A. Shvedov, "A new approach to radioactive waste self-burial using high penetrating radiation", *Journal of Nuclear Science & Technology*, vol. 2018, no. 2, pp. 971–978, 2018. DOI: 10.1080/00223131.2018.1461695.

[12] H. M. Jol, *Ground Penetrating Radar: Theory and Applications*. Elsevier Science, 2009.

[13] L. B. Volkomirskaya, O. A. Gulevich, V. V. Varenkov *et al*., "Requirements for the performance of a ground-penetrating radar system in searching for cavities", *Russian Geology & Geophysics*, vol. 59, no. 4, pp. 438–447, 2018. DOI: 10.1016/j.rgg.2017.05.004.

[14] W.-T. Hong and J.-S. Lee "Estimation of ground cavity configurations using ground penetrating radar and time domain reflectometry", *Natural Hazards*, vol. 92, no. 3, pp. 1789–1807, 2018. DOI: 10.1007/s11069-018-3278-z.

[15] A. Costall and B. Harris, "Rapid estimation of volumetric groundwater recharge in the Vadose Zone via Ground Penetrating Radar", in *Aseg Extended Abstracts*, vol 2018, no. 1, 2018. DOI: 10.1071/ASEG2018abP091.

[16] F. Hui, Zh. Liu, X. Guo X *et al*., "Double-frequency ground penetrating radar for measurement of ice thickness and water depth in rivers and canals: Development, verification and application", *Cold Regions Science & Technology*, vol. 154, pp. 85–94, 2018. DOI: 10.1016/j.coldregions.2018.06.017.

[17] H. Mansor, N. Rosli, N. A. Ismail, M. Saidin, and S. S. K. Masnan, "Mapping subsurface structure at Guar Kepah by using Ground Penetrating Radar", *Journal of Physics: Conference Series*, vol. 995, conference 1, 2018. DOI: 10.1088/1742-6596/995/1/012081.

[18] S. Fontul, M. Solla, H. Cruz, J. S. Machado, and L. Pajewski, "Ground Penetrating Radar investigations in the Noble Hall of São Carlos Theater in Lisbon, Portugal", *Surveys in Geophysics*, vol. 39, no. 6, pp. 1125–1147, 2018. DOI: 10.1007/s10712-018-9477-z.

[19] P. Xie, H. Wen, P. Xiao, and Y. Zhang, "Evaluation of ground-penetrating radar (GPR) and geology survey for slope stability study in mantled karst region", *Environmental Earth Sciences*, vol. 77, no. 4, pp. 122, 2018. DOI: 10.1007/s12665-018-7306-9.

[20] R. Persico, Introduction to Ground Penetrating Radar: Inverse Scattering and Data Processing. Wiley-IEEE Press, 2014. DOI: 10.1002/9781118835647.

[21] X. Lu, A. Song, R. Qian, and L. Liu, "Anisotropic reverse-time migration of Ground-Penetrating Radar data collected on the Sand Dunes in the Badain Jaran Desert", *IEEE Journal of Selected Topics in Applied Earth Observations & Remote Sensing*, vol. 11, no. 2, pp. 647–654, 2018. DOI: 10.1109/JSTARS.2017.2787671.

[22] S. L. Kenady, K. M. Lowe, and S. Ulm, "Determining the boundaries, structure and volume of buried shell matrix deposits using ground-penetrating radar: A case study from northern Australia", *Journal of Archaeological Science Reports*, vol. 17, pp. 538–549, 2018. DOI: 10.1016/j.jasrep.2017.12.015.

[23] A. Janeliauskas, V. Markevicius, D. Navikas, D. Andriukaitis, A. Valinevicius, M. Zilys, "Initial Design and Quick Analysis of SAW Ultra–Wideband HFM Transducers", *Radioengineering*, vol. 26, no. 3, pp. 682–690. DOI: 10.13164/re.2017.0682.

[24] D. M. Sullivan, *Electromagnetic Simulation Using the FDTD Method*. Wiley, Second Edition, 2013. DOI: 10.1002/9781118646700.

[25] X.-K. Wei, W. Shao, Sh. Ding, and B.-Z. Wang, "Hybrid sub-gridded ADE-FDTD method for modeling ground-penetrating radar on dispersive soils", *Journal of Electromagnetic Waves and Applications*, vol. 32, no. 11, pp. 1416–1426, 2018. DOI: 10.1080/09205071.2018.1439775.